Revista Mexicana de Astronomía y Astrofísica, **60**, 277–292 (2024)

https://doi.org/10.22201/ia.01851101p.2024.60.02.06

LONG TERM CCD PHOTOMETRY OF THE DISTANT CLUSTER NGC2419: THE CMD REVISITED

A. Arellano Ferro[1], S. Muneer[2], Sunetra Giridhar[2], I. Bustos Fierro[3], M. A. Yepez[1,4], G. A. García Pérez[5], and G. Rios Segura[5]

Received March 3 2024; accepted May 1 2024

ABSTRACT

Employing *VI* images of NGC 2419 acquired over 17 years, light curves for most of the known variables in the field of the cluster are produced. A cluster membership analysis for about 3100 stars in the cluster field with proper motions from *Gaia*-DR3 revealed the presence of member stars as far as 140 pc from the cluster center and enabled the construction of a cleaner CMD free of field stars. It was found that RRab and RRc stars share the inter-order region in the instability strip, which is unusual for OoII clusters. Theoretical considerations confirm that Pop II cepheids are descendants of extreme ZAHB blue tail stars with very thin envelopes of about 10% of the total mass. Member RR Lyrae stars were employed to calculate independent estimates of the mean cluster metallicity and distance; we found $[\mathrm{Fe/H}]_{\mathrm{UV}} = -1.90 \pm 0.27$ and $D = 86.3 \pm 5.0$ kpc from the RRab and $[\mathrm{Fe/H}]_{\mathrm{UV}} = -1.88 \pm 0.30$ and $D = 83.1 \pm 8.1$ kpc from the RRc light curves.

RESUMEN

Con imágenes CCD *VI* del cúmulo globular NGC 2419, obtenidas durante 17 años, hemos construido curvas de luz de gran parte de las estrellas variables en el campo del cúmulo. A partir de un análisis de membresía basado en los movimientos propios de *Gaia*-DR3 de 3100 estrellas, detectamos miembros a distancias de 140 pc del centro del cúmulo, y construimos un diagrama color-magnitud libre de estrellas de campo. Encontramos que los dos modos de pulsación RRab y RRc comparten la región bimodal de la zona de inestabilidad, lo cual es inesperado en cúmulos Oo II. Nuestros modelos confirman que las estrellas cefeidas de Pob II provienen del extremo azul de la ZAHB con envolventes muy delgadas, de ≈10% de la masa total. A partir de estrellas RR Lyrae miembros calculamos la metalicidad y distancia medias del cúmulo $[\mathrm{Fe/H}]_{\mathrm{UV}} = -1.90 \pm 0.27$ y $D = 86.3 \pm 5.0$ kpc para estrellas RRab, y $[\mathrm{Fe/H}]_{\mathrm{UV}} = -1.88 \pm 0.30$ y $D = 83.1 \pm 8.1$ kpc para estrellas RRc.

Key Words: globular clusters: general — globular clusters: individual: NGC 2419 — stars: distances — stars: fundamental parameters — stars: horizontal branch — stars: variables: RR Lyrae

1. INTRODUCTION

NGC 2419 (C0734+390 in the IAU nomenclature) ($\alpha = 07^{\mathrm{h}}38^{\mathrm{m}}08.47^{\mathrm{s}}$, $\delta = +38°52'56.8''$, J2000; $l = 180.37°$, $b = +25.24°$) is a large and very luminous globular cluster at about 80 kpc from the Galactic center and hence it is among the most distant clusters in the outer halo of our Galaxy. It is noted for being a very loose or extended system given its brightness M_V and half-light radius, which led van den Bergh & Mackey (2004) to suggest its extra galactic origin, and the likelihood of it being a

[1]Instituto de Astronomía, Universidad Nacional Autónoma de México, Ciudad Universitaria, C.P. 04510, México.
[2]Indian Institute of Astrophysics, Bangalore, India.
[3]Observatorio Astronómico, Universidad Nacional de Córdoba, Córdoba C.P. 5000, Argentina.
[4]Instituto Nacional de Astrofísica, Óptica y Electrónica (INAOE), Luis Enrique Erro No.1, Tonantzintla, Pue., C.P. 72840, México.
[5]Facultad de Física, Universidad Veracruzana, Xalapa, México.

stripped core of a former spheroidal dwarf galaxy. These suggestions however have not been supported by Ripepi et al. (2007) on the ground of the following arguments: the cluster is of the Oo II type while extra galactic clusters and dwarf galaxies reside within the Oosterhoff gap (Catelan 2009); the lack of substructures in the main sequence bellow the TO (i.e. lack of multiple populations); the thinness of the red giant branch (ruling out multiple chemical compositions among cluster stars); and the apparent absence of extra-tidal structures. In Ripepi et al's opinion NGC 2419 is a normal metal-poor Galactic globular cluster.

The variable star population of NGC 2419 is quite rich. There are 101 variables registered in the Catalogue of Variable Stars in Globular Clusters (CVSGC) (Clement et al. 2001), 75 of which are RR Lyrae, 1 Pop II or CW star, 12 SX Phe, 5 long-period red giants, 3 eclipsing binaries, 2 δ Scuti stars and 3 non-classified. A thorough analysis of these variable stars, based on high-quality images from the HST, and from two large ground telescopes; the Galileo (TNG) 3.5 and the Subaru 8.2m, was carried out by Di Criscienzo et al. (2011).

Our team has obtained *VI* CCD images of NGC 2419 between 2005 and 2022 for a total of 405 and 327 in V and I respectively, using the 2m telescope of Indian Astronomical Observatory (IAO). Naturally the depth and accuracy of our photometry is not comparable to that used by Di Criscienzo et al. (2011), and due to crowding we were not able to recover the light curves for all known variables. It may seem pretentious to draw conclusions from RR Lyrae stars at $V \sim 20.5$, which nears the faint limit of our data. Nevertheless, we can use our photometry to provide a new discussion of the cluster membership of the stars in the field of our images, particularly those of variable nature, and provide independent estimates for the mean cluster reddening, average metallicity and distance.

Our approach to the determination of mean M_V and [Fe/H] of RRL stars, is the Fourier light curve decomposition, of both the fundamental mode and first overtone pulsators RRab and RRc respectively. This, and the employment of well established semi-empirical calibrations and their zero points between the Fourier parameters and the physical quantities, provide individual stellar estimations of the distance and [Fe/H]; hence, the average of these values for tested cluster member variables leads to proper average values for the parent cluster. The present paper is a report of our results.

TABLE 1

LOG OF OBSERVATIONS OF NGC 2419

Date	N_V	t_V(s)	N_I	t_I(s)	Mean seeing ($''$)
01/04/2005	7	600	-	-	1.9
02/04/2005	8	600	-	-	1.7
03/04/2005	11	600	-	-	1.9
19/01/2006	14	600	-	-	3.4
09/03/2007	8	600	-	-	2.0
10/03/2007	18	600	-	-	2.7
10/04/2007	10	600	-	-	2.0
11/04/2007	13	600	-	-	2.0
07/01/2009	5	300-600	2	300	1.7
08/01/2009	2	600	2	300	2.3
15/12/2011	3	450-500	4	100-150	3.5
16/12/2011	7	400-450	7	120-150	2.8
17/12/2011	2	380-420	4	110-120	2.7
05/02/2012	22	180-300	20	90	2.2
28/02/2012	32	180-200	35	80-100	2.1
29/02/2012	16	250-450	17	80-250	2.8
01/03/2012	11	180-300	12	80-150	2.7
19/01/2013	25	150-400	27	75-150	2.1
20/01/2013	41	170-210	44	80-100	2.2
21/01/2013	3	180	5	80	2.4
04/03/2013	6	125-150	6	65-85	1.8
01/02/2017	14	180	13	80	2.5
02/02/2017	14	180	13	80	2.7
16/02/2020	16	200	16	100	2.8
17/02/2020	8	200	8	100	2.4
19/03/2021	12	200	12	100	1.9
04/11/2021	27	200	28	100	2.6
12/02/2021	10	200	10	100	2.0
03/01/2022	8	200	8	100	2.9
31/01/2022	32	200	34	100	2.4
Total:	405		327		

Columns N_V and N_I give the number of images taken with the V and I filters respectively. Columns t_V and t_I provide the exposure time, or range of exposure times. In the last column the average seeing is listed.

2. OBSERVATIONS AND IMAGE REDUCTIONS

2.1. *Observations*

All observations were carried out with the Himalayan Chandra 2.0m Telescope of the Indian Astrophysical Observatory (IAO) at Hanle, in the Indian Himalayan range at about 4500 m above sea level. The detailed log of the observations is given in Table 1, where exposure times and estimations of the prevailing nightly average seeing are indicated. A total of 405 and 327 images in V and I were secured in a time span of seventeen years.

2.2. *Transformation to the Standard System*

The instrumental photometry was transformed to the standard Johnson-Kron-Cousins photometric system (Landolt 1992) *VI*, using local standard stars in the fields of the target clusters. These standard stars have been taken from the extensive collection of Stetson (2000)[6]. We found 554 standard stars

[6] `https://www.canfar.net/storage/list/STETSON/Standards`.

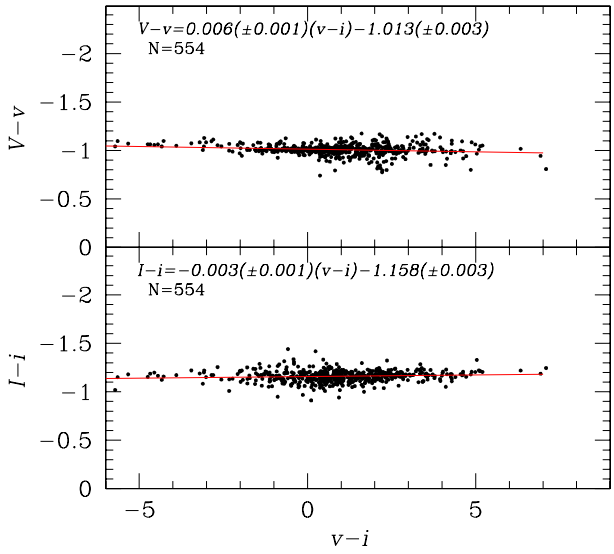

Fig. 1. Transformation relationship between instrumental and standard photometric systems. These equations were calculated using 554 local standard stars from the collection of Stetson (2000). The colour figure can be viewed online.

with instrumental light curves in the field of our images. The standard minus instrumental magnitudes and the light dependence with the $(v - i)$ colour is displayed in Figure 1. The corresponding transformation equations are also given in the figure.

2.3. *Difference Image Analysis*

All the image photometric treatment has been performed using the Difference Image Analysis using the *DanDIA* pipeline (Bramich 2008; Bramich et al. 2013, 2015). The approach and its caveats have been described in detailed by Bramich et al. (2011).

3. STELLAR MEMBERSHIP ANALYSIS

Distinguishing the true cluster members from the field stars projected on the field of view of a cluster is relevant since one is interested in a clean CMD that represents the structure of the system. Presently, this challenge is on reach given the high quality proper motions available in the *Gaia* mission (Gaia Collaboration et al. 2023).

The method developed by Bustos Fierro & Calderón (2019) to determine the stellar membership is based on a two step approach: (1) it finds groups of stars with similar characteristics in the four-dimensional space of the gnomonic coordinates (X_t,Y_t) and proper motions ($\mu_{\alpha*}$,μ_δ) employing the BIRCH clustering algorithm (Zhang et al. 1996) and (2) in order to extract likely members that were missed in the first stage, the analysis of the projected distribution of stars with different proper motions around the mean proper motion of the cluster is performed.

This method was applied to the stars within a radius of 15 arc minutes from the center of NGC 2419. This field contains 3965 *Gaia* sources but only 3129 have a measurement of the proper motion, 1584 of which were found to be likely cluster members. In Figure 2 the corresponding Vector Point Diagram (VPD) and colour-magnitude diagram (CMD) showing the cluster member and field stars are shown. The farthest member from the center is about 6 arc minutes away which, at a distance of 84.0 kpc (see our distance determination in § 7) corresponds to a distance of about 140 pc. In spite of its half-light radius at about 17.9 pc, comparable to other clusters in the halo (van den Bergh & Mackey 2004), these star members at such large distances are the indication of the extended halo that led van den Bergh & Mackey (2004) to suggest its extra galactic origin and presently being the remains of a former dwarf galaxy tidally stripped by the Milky Way. In Figure 3, the radial distance distribution of member stars in NGC 2419 is displayed and shows its extended nature. For comparison we included the similar distribution of large halo cluster NGC 1851. The membership analysis reveals the bound nature of a subtle cluster halo as large as 140 pc from the cluster center.

We have been able to obtain *VI* photometry for 1107 point sources in the field of our images. These light curves include 74 of the known variables in the cluster (Clement et al. 2001), and the general data for these variables is included in Table 2. A CMD with these variables identified has been produced and will be discussed in the following sections.

4. VARIABLE STARS MEASURED IN THE PRESENT STUDY

Given the size of our telescope and sky conditions at the time of the observations which limited the deepness and resolution of our imaging data, some of the well known variables remain blended and it was not possible to measure them well. It should be noted that the HB level of this distant cluster is fainter than 20th magnitude, which is close to the faint limit of our capabilities. Variables in Table 2 are mostly RR Lyrae (RRab and RRc), but also a sample of red giant branch variables (RGBs) is available, plus one W Vir (V18) and one double mode or RRd star (V39). The identifications of these variables are given in the charts of Figure 4. Their

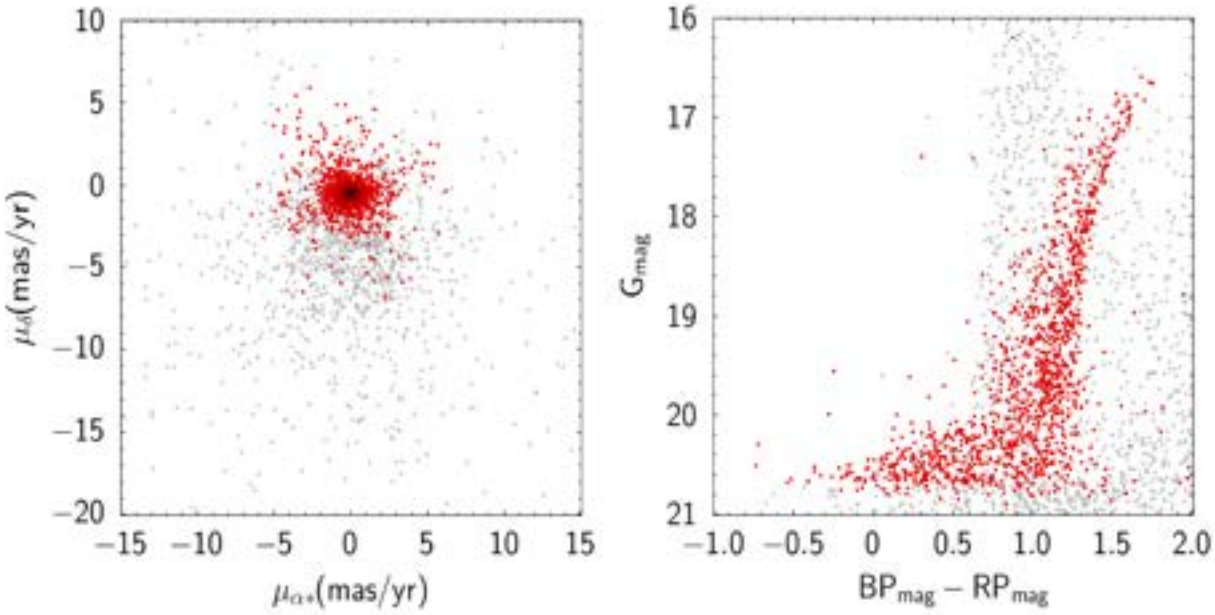

Fig. 2. *Gaia*-DR3 VPD (left panel) and CMD (right panel) of the cluster NGC 2419. Red and gray points correspond to likely cluster members and field stars respectively, determined as described in § 3. A total of 3965 *Gaia* point sources within 15 arc minutes are displayed, while 1584 were found to be cluster members. The colour figure can be viewed online.

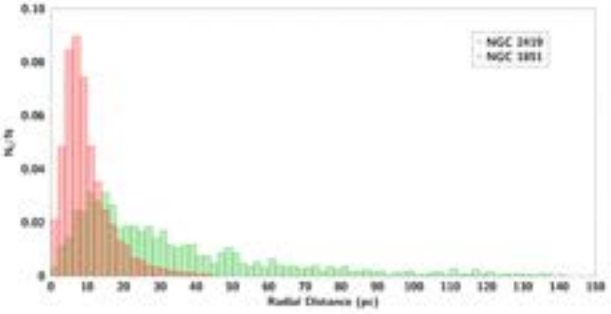

Fig. 3. Star members distribution of the extended cluster NGC 2419 compared with the large halo cluster NGC 1851. The horizontal axis represents the radial distance projected on the plane of the sky. The colour figure can be viewed online.

light curves are displayed in the Appendix, where we have distinguished the data from the several observing runs.

5. THE OOSTERHOFF TYPE OF NGC 2419

Given its low metallicity the cluster likely belongs to the Oo II type. This is in fact confirmed by the period average of its RRab and RRc stars of 0.665 d and 0.343 d respectively. The log P - Amplitude diagram (Bailey's diagram) is shown in Figure 5. It is clear that the distribution of stars, particularly that of the RRab, falls towards the sequences of evolved star (Cacciari et al. 2005) which is the characteristic of Oo II type clusters.

6. ON THE CLUSTER REDDENING

Given its Galactic location, NGC 2419 is not much affected by interstellar reddening. To estimate the colour excess of individual RRab stars, we have taken advantage of the fact that the $V - I$ colour curve of RRab stars is constant near its minimum, between the phases 0.5 and 0.8 (Sturch 1966). By employing the calibration of $(V - I)_{0,min} = 0.58 \pm 0.02$ (Guldenschuh et al. 2005), we calculated the average colour excess for 12 cluster member RRab and found $E(B - V) = 0.07 \pm 0.07$. This average is comparable with the predicted values from the calibrations of Schlafly & Finkbeiner (2011) and Schlegel et al. (1998), 0.052 ± 0.001 and 0.061 ± 0.001 respectively. In this work we adopted $E(B - V) = 0.06$ or $E(V - I) = 1.259 \times E(B - V)$, which leads to $E(V - I) = 0.08$.

7. PHYSICAL PARAMETERS OF THE RR LYRAE STARS FROM THE LIGHT CURVES FOURIER DECOMPOSITION

Our approach to the calculation of relevant stellar physical parameters for the RR Lyrae stars is

TABLE 2

GENERAL DATA OF THE VARIABLES OF THE FOV FOR NGC 2419

Variable	Type	$<V>$ (mag)	$<I>$ (mag)	A_V (mag)	A_I (mag)	Period (days)	HJD_{max} (d+2450000)	RA (J2000.0)	Dec. (J2000.0)	Membership (m/f/un)
					RRab					
V2	RRab	19.675	18.927	0.772	-	0.792335	4169.173	07:38:07.96	+38:52:33.7	m
V3	RRab	20.370	19.811	1.163	0.713	0.625995	9293.321	07:38:12.71	+38:52:27.4	m
V5	RRab	19.895	19.171	0.520	0.342	0.655855	9293.166	07:38:11.14	+38:53:38.8	m
V7	RRab	20.484	19.886	1.341	0.830	0.627353	6312.483	07:38:16.19	+38:54:18.8	m
V9	RRab	20.316	19.614	1.239	0.751	0.644727	4202.120	07:38:05.63	+38:54:21.2	m
V11	RRab	20.436	20.031	1.097	0.931	0.589179	4170.333	07:38:16.43	+38:52:42.3	m
V12	RRab	20.405	19.871	1.087	0.687	0.661853	9611.116	07:38:19.79	+38:54:41.0	m
V13	RRab	20.425	19.849	1.051	0.687	0.640	4169.334	07:38:16.93	+38:52:40.2	m
V14	RRab	20.257	19.777	1.310	1.003	0.741	9258.370	07:37:58.39	+38:52:42.3	m
V15	RRab	20.438	19.846	1.265	0.813	0.640	9293.166	07:38:13.66	+38:53:30.6	m
V16	RRab	20.202	-	1.139	-	0.666	4202.120	07:38:12.38	+38:54:03.4	m
V17	RRab	20.406	19.822	0.979	0.619	0.649	4201.162	07:38:17.74	+38:54:41.0	m
V19	RRab	20.434	19.890	1.303	0.866	0.703	9258.370	07:37:59.02	+38:52:15.0	m
V21	RRab	20.318	19.830	1.497	0.690	0.686	9293.166	07:38:03.58	+38:53:23.7	m
V22	RRab	20.404	-	1.123	-	0.577	6312.478	07:38:17.65	+38:52:44.4	m
V23	RRab	19.976	19.476	0.996	-	0.626	5988.205	07:38:10.70	+38:54:10.7	m
V24	RRab	20.427	19.743	0.869	0.799	0.653	4169.276	07:37:55.61	+38:52:45.7	m
V25	RRab	20.330	19.595	0.851	0.536	0.636	3464.280	07:38:03.28	+38:53:31.7	m
V26	RRab	19.609	18.958	0.580	0.373	0.664	4201.163	07:38:02.20	+38:52:03.2	m
V29	RRab	20.349	19.909	0.759	0.598	0.726	3464.173	07:38:03.26	+38:52:46.9	m
V30	RRab	20.600	-	1.152	-	0.584	4170.189	07:38:06.09	+38:53:16.2	m
V32	RRab	20.188	19.443	0.729	0.615	0.642	4170.230	07:38:06.70	+38:53:40.8	m
V35	RRab	20.797	-	1.627	-	0.677	4839.390	07:38:12.01	+38:52:59.9	m
V36	RRab	20.310	-	0.708	-	0.648	9611.423	07:38:10.30	+38:53:35.3	m
V37	RRab	19.361	18.467	0.184	0.226	0.661	4170.257	07:38:11.20	+38:53:09.1	un
V40	RRab	18.930	17.989	0.229	0.195	0.576	6312.400	07:38:13.09	+38:52:47.2	un
V42	RRab	19.787	-	0.277	-	0.775	5963.194	07:38:08.72	+38:52:45.7	un
V57	RRab	20.041	19.516	0.812	0.483	0.736	5963.078	07:38:06.00	+38:52:42.7	m
V59	RRab	20.258	-	0.585	-	0.829	5963.161	07:38:10.43	+38:53:09.5	m
V64	RRab	20.385	19.638	0.337	0.449	0.781	4170.333	07:38:10.29	+38:52:16.3	m
					RRc					
V4	RRc	20.420	19.917	0.403	0.380	0.392	6313.385	07:38:15.13	+38:52:35.1	m
V6	RRc	20.349	-	0.553	-	0.372	3463.242	07:38:12.89	+38:50:43.8	m
V27	RRc	20.454	-	0.311	-	0.342	9258.425	07:38:09.78	+38:51:09.0	m
V31	RRc	20.297	-	0.509	-	0.388	9293.285	07:38:21.24	+38:50:22.9	m
V33	RRc	20.604	-	0.427	-	0.303	5963.118	07:38:12.27	+38:52:33.9	m
V34	RRc	20.437	-	0.531	-	0.399	4170.119	07:38:10.34	+38:55:29.1	m
V38	RRc	18.748	17.819	0.134	0.162	0.364	5963.161	07:38:08.13	+38:52:03.9	un
V41	RRc	19.324	18.629	0.167	0.154	0.396	4202.187	07:38:07.20	+38:53:23.1	un
V48	RRc	19.452	18.241	0.218	0.219	0.375	6356.102	07:38:10.04	+38:52:41.2	un
V51	RRc	19.914	19.307	0.266	0.417	0.348	4839.375	07:38:06.19	+38:52:57.5	un
V55	RRc	20.392	-	0.409	-	0.378	4839.375	07:38:05.99	+38:52:59.6	m
V56	RRc	19.415	19.154	0.108	0.373	0.333	5963.117	07:38:07.99	+38:52:24.7	un
V60	RRc	20.376	-	0.362	-	0.390	6313.478	07:38:06.66	+38:53:18.8	m
V66	RRc	20.515	-	0.419	-	0.387	6313.156	07:38:11.60	+38:53:10.5	m
V67	RRc	19.978	-	0.305	-	0.348	5963.118	07:38:10.97	+38:53:23.5	m
V68	RRc	20.333	-	0.435	-	0.365	6313.454	07:38:12.15	+38:52:49.0	m
V69	RRc	20.109	19.441	0..335	0.386	0.344	5986.225	07:38:10.64	+38:53:37.7	un
V72	RRc	20.412	19.700	0.426	0.350	0.415	5912.464	07:38:09.92	+38:53:49.5	m

Columns 3 and 4 list mean magnitudes, Columns 5 and 6 show light curve amplitudes. Column 11 indicates the cluster membership status; m - members, f - field, un - unknown.

TABLE 2. CONTINUED

Variable	Type	$<V>$ (mag)	$<I>$ (mag)	A_V (mag)	A_I (mag)	Period (days)	HJD_{max} (d+2450000)	RA (J2000.0)	Dec. (J2000.0)	Memb (m/f/un)
V74	RRc	20.598	-	0.206	-	0.309	5963.118	07:38:13.78	+38:52:47.9	m
V75	RRc	20.288	-	0.429	-	0.324	4840.363	07:38:03.54	+38:52:16.9	m
V76	RRc	20.128	19.579	0.275	0.302	0.324	5986.267	07:38:12.11	+38:51:59.2	m
V77	RRc	20.298	-	0.332	-	0.381	5963.117	07:38:13.14	+38:52:08.2	m
V82	RRc	19.911	19.594	0.205	0.327	0.343	9293.289	07:38:13.85	+38:53:37.3	m
V84	RRc	20.046	19.165	0.287	0.301	0.329	5986.225	07:38:01.46	+38:53:12.0	m
V89	RRc	20.273	-	0.283	-	0.287	5963.118	07:38:19.78	+38:55:07.4	f
V90	RRc	20.354	-	0.328	-	0.391	5963.124	07:38:23.14	+38:54:11.6	m
					RRd					
V39	RRd	20.335	-	-	-	0.814	5963.181	07:38:10.72	+38:50:51.1	m
					RGBs					
V1	RGB	17.188	15.664	0.451	0.472	193.850	5963.161	07:38:11.61	+38:51:59.0	m
V8	RGB	17.301	15.887	0.603	0.613	16.350	9258.370	07:38:06.84	+38:53:34.1	m
V10	RGB	17.085	15.552	0.466	0.374	20.800	7786.166	07:38:09.89	+38:52:01.1	m
V20	RGB	17.425	16.680	0.427	0.528	48.980	5963.161	07:38:05.96	+38:53:38.2	m
V86	RGB	17.343	15.932	0.548	0.418	49.860	5963.161	07:38:19.62	+38:53:15.7	m
					V Vir					
V18	W VIR	18.837	18.207	0.412	0.725	1.579	4202.120	07:38:07.17	+38:54:46.8	m

Columns 3 and 4 list mean magnitudes, Columns 5 and 6 show light curve amplitudes. Column 11 indicates the cluster membership status; m - members, f - field, un - unknown.

via the Fourier decomposition of their V-band light curves. Of particular interest are the mean [Fe/H] and M_V of the RR Lyrae sample, as they are good representations of the mean cluster metallicity and distance.

The Fourier decomposition is performed by fitting the observed light curve with a Fourier series model of the form:

$$m(t) = A_0 + \sum_{k=1}^{N} A_k \cos\,(\frac{2\pi}{P}\ k\ (t-E) + \phi_k), \quad (1)$$

where $m(t)$ is the magnitude at time t, P is the period, and E is the epoch. A linear minimization routine is used to derive the best-fit values of the amplitudes A_k and phases ϕ_k of the sinusoidal components. From the amplitudes and phases of the harmonics in eq. 1, the Fourier parameters, defined as $\phi_{ij} = j\phi_i - i\phi_j$, and $R_{ij} = A_i/A_j$, are computed.

Subsequently, the low-order Fourier parameters can be used in combination with semi-empirical calibrations to calculate [Fe/H] and M_V. The employed calibrations for the mass, $T_{\rm eff}$, and radii are summarized in the papers by Arellano Ferro et al. (2010) and Arellano Ferro et al. (2011), while the calibrations for [Fe/H] and M_V and their zero points are most recently discussed by Arellano Ferro (2022) and Arellano Ferro (2024).

7.1. *Physical Parameters of RR Lyrae Stars*

The Fourier coefficients for the RRab and RRc stars were calculated for the stars that we were able to measure. For the sake of briefness these are not specifically given in this paper but they are available on request. These coefficients were then used in the cited calibrations to calculate the individual physical parameters, which are reported in Table 3. The average [Fe/H] and M_V (hence distance), should be representative of the parent cluster. It should be noted that the calibrations render the value $[{\rm Fe/H}]_{\rm ZW}$, i.e. in the metallicity scale of Zinn & West (1984) which can be transformed into the spectroscopic scale of Carretta et al. (2009), via the equation; $[{\rm Fe/H}]_{\rm UVES} = -0.413 + 0.130\ [{\rm Fe/H}]_{\rm ZW} - 0.356\ [{\rm Fe/H}]^2_{\rm ZW}$.

We found averages $[{\rm Fe/H}]_{\rm ZW} = -1.86 \pm 0.18$, $[{\rm Fe/H}]_{\rm UV} = -1.90 \pm 0.27$ and $D = 86.3 \pm 5.0$ kpc. from the RRab light curves, and $[{\rm Fe/H}]_{\rm ZW} = -1.84 \pm 0.21$, $[{\rm Fe/H}]_{\rm UV} = -1.88 \pm 0.30$ and $D = 83.1 \pm 8.1$ kpc from the RRc data. Emphasis should be made that, coming from independent calibrations with different calibrators, the results for the RRab and RRc stars are also fully independent. Still there is a very satisfactory agreement. These values can be compared with the value quoted $[{\rm Fe/H}]_{Spec} = -2.2$ in the spectroscopic scale (Carretta et al. 2009), and the critical literature mean distance $D = 88.47 \pm 2.40$ kpc estimated by Baumgardt & Vasiliev (2021). Thus, the agreement of our metallicity and distance determinations for NGC 2419 with this canonical values, cannot be better.

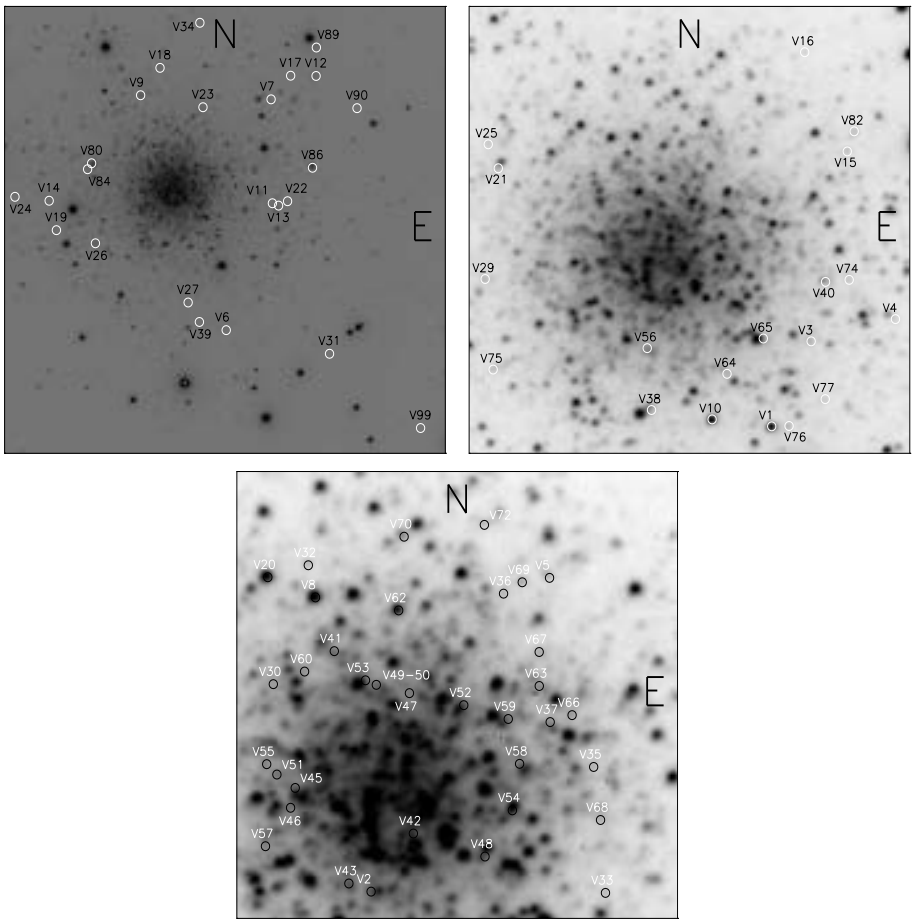

Fig. 4. Identification chart of variable stars in the field of NGC 2419. The approximate size of each images is 6.9×6.9, 2.5×2.5 and 1.6×1.6 square arc minutes.

8. DISCUSSION: THE COLOR MAGNITUDE DIAGRAM

In Figure 6 we display two versions of the observed CMD. The panel on the left shows the stellar distribution of every point source that we were able to measure in our collection of *VI* images. This includes cluster member stars as well as field stars. Through the membership analysis described in § 3, we could distinguish the most likely cluster members (red dots in the figure) from the field stars (small light blue dots). In the right panel, we have plotted only the cluster members and have dereddened the diagram by assuming $E(V-I) = 0.08$. The variable stars contained in Table 4 are plotted with colours according to their pulsational type, as coded in the figure caption. When a variable is found to be a cluster member, the colour symbol has a smaller red dot in the center, otherwise the star had no proper motion reported in *Gaia*-DR3, and hence its membership status is unknown, or it is likely a field star.

We also include in this dereddened diagram the two isochrones from VandenBerg et al. (2014) for ages of 12.5 Gyr (black) and 13.0 Gyr (turquoise) with [Fe/H]= -1.8 and -2.0, respectively. Red ZAHB is from the models built from the Eggleton code (Pols et al. 1997, 1998; Schröder et al. 1997), and calculated by Yepez et al. (2022). The black evolutionary track corresponds to a model with a central core mass of $0.50\,M_{\odot}$ and a thin envelope of $0.04\,M_{\odot}$ and it was selected as it best represents the position of the W Vir star V18 confirming the conclusions reached by Yepez et al. (2022), that type II Cepheids can be interpreted as products of post-HB evolution driven by burning of very low mass hydrogen and helium shells. According to Bono et al. (2020), W Vir stars may be post-early asymptotic giant branch stars (see also the case of the CWB star V81 in NGC 7006 (Arellano Ferro et al. 2023)), although the case of V18 seems more like that of a post-HB which according to the model has taken 114 million years from the HB to reach its present position.

TABLE 3

PHYSICAL PARAMETERS FROM THE MEMBER RR LYRAE FOURIER LIGHT CURVE DECOMPOSITION

ID	$[Fe/H]_{ZW}$	$[Fe/H]_{UVES}$	M_V	$\log T_{\rm eff}$	$\log(L/L_\odot)$	$M/M_\odot$	$D(kpc)$	$R/R_\odot$
				RRab				
V3	-1.78(9)	-1.77(11)	0.51(1)	3.80(2)	1.71(1)	0.73(14)	83.61(43)	6.01(3)
V9	-1.74(9)	-1.77(11)	0.46(1)	3.80(2)	1.73(1)	0.76(15)	83.41(48)	6.19(3)
V12	-2.09(10)	-2.24(15)	0.43(1)	3.80(2)	1.76(1)	0.83(16)	88.37(45)	6.54(3)
V13	-1.69(10)	-1.65(12)	0.50(1)	3.80(2)	1.72(1)	0.73(16)	86.13(44)	6.09(3)
V14	-2.23(10)	-2.47(17)	0.37(1)	3.79(2)	1.79(1)	0.86(20)	84.65(55)	7.06(4)
V15	-1.71(11)	-1.68(13)	0.46(1)	3.80(2)	1.73(1)	0.76(17)	88.41(52)	6.18(3)
V16	-2.05(18)	-2.17(27)	0.34(2)	3.80(3)	1.79(1)	0.89(31)	94.75(1.12)	6.75(7)
V17	-1.91(12)	-1.95(16)	0.45(1)	3.80(2)	1.74(1)	0.78(19)	87.28(62)	6.30(4)
V19	-1.88(12)	-1.92(15)	0.35(1)	3.80(2)	1.78(1)	0.80(19)	92.56(55)	6.65(4)
V21	-1.91(10)	-1.95(13)	0.39(1)	3.80(2)	1.77(1)	0.80(19)	86.50(51)	6.58(3)
V22	-1.79(10)	-1.79(13)	0.47(1)	3.81(3)	1.73(1)	0.80(26)	93.55(68)	5.94(4)
V24	-1.57(15)	-1.50(17)	0.49(1)	3.80(3)	1.72(1)	0.68(24)	86.77(63)	5.99(4)
V25	-1.74(7)	-1.72(8)	0.51(1)	3.80(1)	1.72(1)	0.72(12)	82.27(29)	6.03(2)
V29	-2.12(12)	-2.28(18)	0.40(01)	3.79(1)	1.77(1)	0.84(18)	87.01(46)	6.90(3)
V32	-1.67(9)	-1.62(10)	0.50(1)	3.80(1)	1.72(1)	0.72(15)	77.43(29)	6.04(2)
V57	-1.91(12)	-1.97(16)	0.46(1)	3.79(2)	1.74(1)	0.74(20)	75.11(33)	6.64(3)
V59	-2.51(62)[1]	-2.79(1.11)[1]	0.39(02)	3.78(6)	1.79(1)	0.82(60)	89.19(88)	7.27(6)
Mean	-1.86	-1.90	0.44	3.80	1.75	0.78	86.3	6.42
σ	±0.18	±0.27	±0.5	±0.01	±0.03	±0.03	±5.0	±0.40
				RRc				
V4	-1.71(11)	-1.68(13)	0.51(4)	3.83(1)	1.69(1)	0.46(2)	85.43(14)	4.54(7)
V6	-2.06(7)	-2.19(11)	0.51(4)	4.12(1)	1.70(1)	0.53(2)	85.70(16)	4.63(8)
V27	-1.54(14)	-1.45(16)	0.75(4)	3.84(1)	1.60(2)	0.53(2)	81.09(16)	4.42(8)
V31	-1.61(20)	-1.55(23)	0.48(3)	3.86(1)	1.71(1)	0.48(2)	85.60(14)	4.59(8)
V33	-1.75(39)	-1.74(48)	0.55(8)	3.84(1)	1.68(3)	0.53(5)	92.40(35)	4.91(18)
V34	-1.70(8)	-1.66(10)	0.42(4)	3.86(1)	1.73(2)	0.50(3)	92.44(1.92)	4.78(10)
V55	-1.06(20)[1]	-0.95(15)[1]	0.52(5)	3.87(1)	1.69(2)	0.45(3)	85.79(1.67)	4.39(10)
V60	-1.60(3)	-1.53(3)	0.58(4)	3.86(1)	1.67(2)	0.42(2)	81.37(1.53)	4.37(8)
V66	-1.79(11)	-1.79(14)	0.54(4)	3.86(1)	1.69(2)	0.46(2)	91.17(1.89)	4.51(9)
V67	-1.96(5)	-2.04(7)	0.56(3)	3.86(1)	1.68(1)	0.52(2)	70.60(1.03)	4.46(6)
V68	-2.12(9)	-2.28(14)	0.48(2)	3.85(1)	1.71(1)	0.58(2)	85.95(1.07)	4.74(6)
V72	-2.12(10)	-2.29(15)	0.49(4)	3.85(1)	1.70(2)	0.51(2)	86.02(1.61)	4.87(9)
V74	-2.05(8)	-2.17(12)	0.62(4)	3.85(1)	1.65(1)	0.61(3)	90.07(1.50)	4.40(7)
V75	-1.36(6)[1]	-1.25(6)[1]	0.56(3)	3.87(1)	1.68(1)	0.53(2)	81.04(1.04)	4.27(5)
V76	-1.49(11)	-1.39(12)	0.39(4)	3.86(1)	1.74(1)	0.45(2)	79.03(1.31)	4.85(8)
V77	-1.94(15)	-2.00(21)	0.44(4)	3.84(1)	1.72(1)	0.61(3)	86.16(1.43)	5.09(8)
V84	-2.05(15)	-2.19(22)	0.56(3)	3.86(1)	1.68(1)	0.58(2)	70.47(92)	4.48(6)
V82	-1.77(12)	-1.75(15)	0.77(3)	3.84(1)	1.59(1)	0.49(1)	60.06(75)	4.36(5)
V90	-2.085(24)	-2.23(35)	0.42(4)	3.85(1)	1.73(2)	0.56(3)	88.57(1.83)	4.88(10)
Mean	-1.84	-1.88	0.53	3.86	1.69	0.52	83.1	4.61
σ	±0.21	±0.30	±0.10	±0.01	±0.04	±0.05	±8.1	±0.23

[1]Value not included in the calculation of the mean.

A qualitative comparison of our limited CMD with the deep and detailed CMD, Figure 2 of Di Criscienzo et al. (2011) (hereinafter diC11), leads to the following instructive observations. First, NGC 2419 has a well developed HB blue tail from where V18 has most likely evolved.

Our photometry does not reach these faint regions of the CMD. If we consider the variable star distribution near the HB in diC11 CMD, we may conclude that all RR Lyrae in their study are cluster members. However, diC11 did not perform a membership analysis. In our CMD of Figure 6, sev-

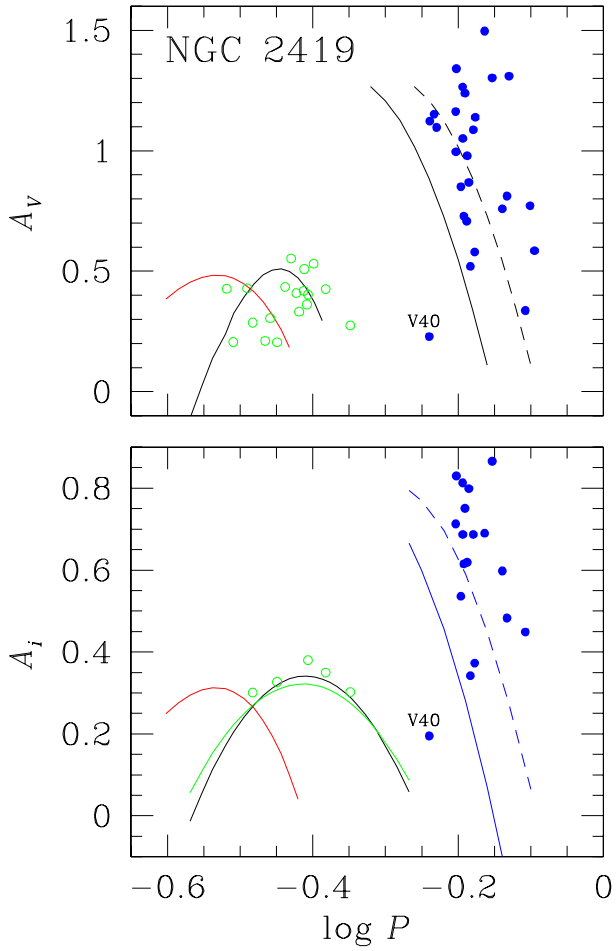

Fig. 5. Period-Amplitude diagram for the RR Lyrae in NGC 2419. Blue and green symbols represent RRab and RRc stars respectively. The star V40 is not a cluster member. In the top panel, the curves to the right are the locy for RRab stars (unevolved continuous and evolved segmented) in M3 according to Cacciari et al. (2005). The black parabola for the RRc stars was calculated by Kunder et al. (2013b) from 14 OoII clusters and Arellano Ferro et al. (2015) calculated the red parabolas from a sample of RRc stars in five OoI clusters. In the bottom panel, the continuous and segmented blue lines were constructed by Kunder et al. (2013a). The black and green parabolas were calculated by Yepez et al. (2020) and Deras et al. (2019) respectively, using 35 RRc stars from eight OoII clusters. The colour figure can be viewed online.

eral RR Lyrae appear noticeably brighter than the HB (e.g. V37, V38, V40, V41, V48, V51, V56 and V69). It is not difficult to corroborate from the identification chart of Figure 4, that these stars are tenants of the cluster central regions and hence are most likely blended, making our photometry further limited and hence producing spurious positions in our CMD. These conditions may have also limited the possibilities of the *Gaia* mission to measure them, as none of them have proper motions reported in *Gaia*-DR3; thus, we have assigned them the unknown (UN) membership status in Table 2. The membership of these variables in NGC 2419 should be corroborated in the future. The rest of the variables in Table 2, all likely members, are distributed closer to the HB with some scatter. This scatter is comparable to that observed in Figure 2 of diC11 if plotted at the same scale; therefore, the RR Lyrae population shows signs of evolution off the ZAHB.

The mass distribution along the ZAHB is determined by the amount of mass lost during the He-flash events at RGB, as it is clearly demonstrated by the models of Silva Aguirre et al. (2008). The more mass is lost, the less massive the star is when settling towards the bluer regions of the ZAHB. This is consistent, for instance, with the fact that bluer (hotter) RRc stars are less massive than redder (cooler) RRab stars. The two modes are in principle separated by the first overtone red edge (FORE) of the instability strip. Depending upon the exact total mass at exhaustion of core-Helium, RRc and RRab stars can either be neatly separated by the FORE or can share the inter-order or bimodal instability strip (i.e. the intersection of the first overtone and fundamental mode instability strips). These concepts are graphically illustrated in Figure 3 of Caputo et al. (1978).

The empirical position of the FORE (Arellano Ferro et al. 2015, 2016) is shown in Figure 6 by two black vertical lines. Also shown are the theoretical borders of the instability strip for the first overtone and fundamental modes from Bono et al. (1994). Note that the theoretical and empirical FORE match very well. It was found by Arellano Ferro et al. (2019) that in all OoII type clusters studied by them, RR Lyrae pulsating modes are well segregated by the FORE, whereas such clear segregation happens only in some OoI clusters, while in others the two modes share the inter-order or "either-or" region. This was interpreted by these authors as indicating that in OoII clusters the RR Lyrae stars always start their ZAHB evolution from less massive bluer stars, while in OoI clusters they exhibit a wider mass distribution, and hence segregation may or may not occur. It remains unclear what physics constrain these two options but it is likely connected with the mass-loss processes during the RGB.

In the case of NGC 2419, the RRc and RRab stars are all mixed across the HB. This can be seen in the CMD of Figure 6, but also in the CMD in Figure 2 of

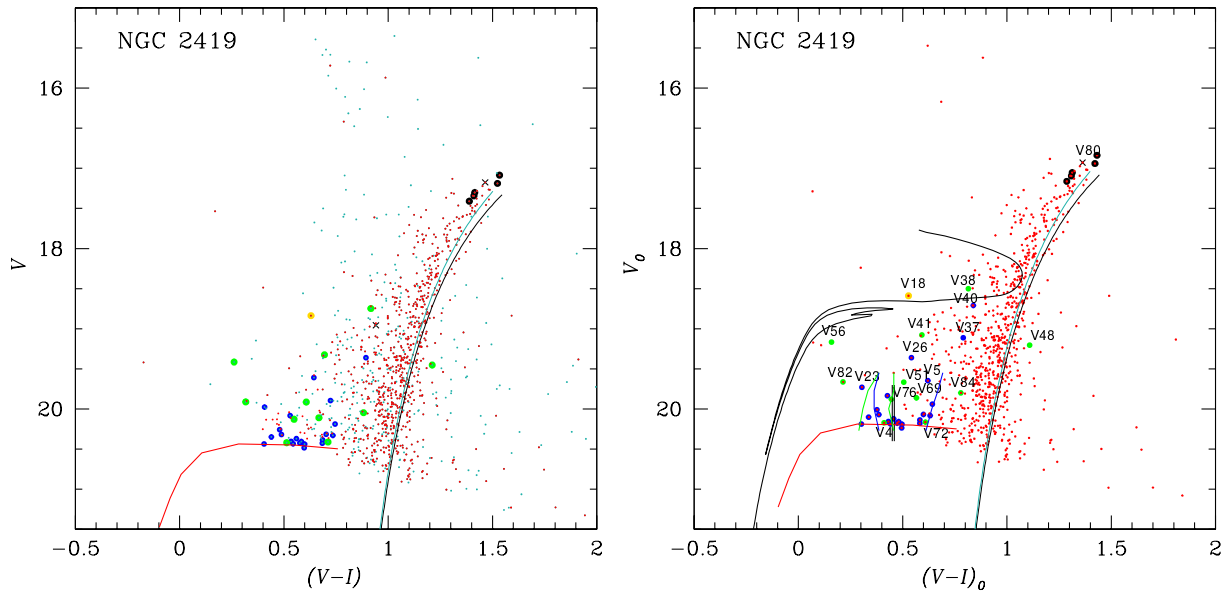

Fig. 6. Observed CMD of NGC 2419. The left panel shows the field stars (small blue dots) and likely cluster member stars (red dots), according to our membership analysis. The right panel shows only the member stars in the dereddened plane. We use $E(B-V) = 0.08$. Blue and green circles represent RRab and RRc stars, respectively. Black circles are used for SR stars. The only CW star is the yellow circle. Black X corresponds to V80, whose variability we could not confirm. The vertical black lines at the ZAHB mark the empirical red edge of the first overtone instability strip (Arellano Ferro et al. 2015, 2016). Also shown are the theoretical fundamental (blue lines) and first overtone (green lines) instability strip borders from Bono et al. (1994). Isochrones are from VandenBerg et al. (2014) for an age of 12.5 Gyr (black) and 13.0 Gyr (turquoise) with [Fe/H]= -1.8 and -2.0, respectively. Red ZAHB is from the models built from the Eggleton code (Pols et al. 1997, 1998; Schröder et al. 1997), and was calculated by Yepez et al. (2022). The black evolutionary track corresponds to a model of total mass 0.54 $M_\odot$ and a core of 0.50 $M_\odot$. These very thin envelope models explain well type II Cepheids such as V18 (Yepez et al. 2022). The colour figure can be viewed online.

diC11. For a Oo II cluster, the location of RRab stars in the inter-order region is contrary to the argument given in the earlier paragraph. Hence, NGC 2419 is an unconventional Oo II cluster exhibiting mixing of the modes in the instability strip.

9. CONCLUSIONS

Using the *Gaia*-DR3 proper motions of stars in the field of NGC 2419, we have been able to confirm the membership of most of the variables known in the cluster. Several of the known variables are in crowded environments and, due to blending with neighbours, we were not able to resolve them; thus, they may appear in odd positions in the CMD. These stars also lack *Gaia*-DR3 proper motion data; thus, we cannot confirm their membership status (e.g. V38, V41, V48, V51, V56, V69). V89, with a proper motion measurement, was found to be a likely field star.

The radial distribution of member stars, clearly demonstrates the extended reach of the cluster to distances of about 140 pc, making of NGC 2419 one of the largest clusters in the Galaxy.

From the Fourier light curve decomposition of clearly resolved RR Lyrae stars, we determined the average metallicity and distance $[\mathrm{Fe/H}]_{\mathrm{UV}} = -1.90 \pm 0.27$ and $D = 86.3 \pm 5.0$ kpc from the RRab light curves and $[\mathrm{Fe/H}]_{\mathrm{UV}} = -1.88 \pm 0.30$ and $D = 83.1 \pm 8.1$ kpc from the RRc stars. These determinations are in excellent agreement with the well established results $[\mathrm{Fe/H}]_{Spec} = -2.2$ (Carretta et al. 2009), and $D = 88.47 \pm 2.40$ kpc (Baumgardt & Vasiliev 2021).

Our post He-flash models show that the W Virginis star V18 has evolved from a ZAHB blue tail progenitor with a very thin shell; this progenitor has a total mass of 0.54 $M_\odot$ but a shell of only 0.04 $M_\odot$. These results confirm the conclusions from Deras et al. (2022) for the Pop II cepheids of M56 or from Yepez et al. (2022) for M14, that thin shells are a required condition for the generation of Pop II cepheid pulsations.

AAF is grateful to the Indian Institute of Astrophysics, for warm hospitality during the writing of

this work. AAF also thankfully acknowledges the sabbatical support granted by the program PASPA of the DGAPA-UNAM. The present project has benefited from the support of DGAPA-UNAM through projects IG100620 and IN103024. The permanent help received from the IA-UNAM librarian, Beatriz Juárez Santamaría, with the bibliographical material needed for this work is fully acknowledged. We are thankful to the IAO TACs for the telescope time allocations over 17 years and to the supporting staff at the Hanle (IAO) and Hosakote (CREST) observing stations. The facilities at IAO and CREST are operated by the Indian Institute of Astrophysics, Bangalore.

A. APPENDIX

A.1. *Light Curves of Measured Variable Stars*

The light curves of all variables resolved in our photometry are displayed in Figures 7, 8, 9 and 10 for the RRab, RRc, RGBs and CW respectively.

A.2. *Comments on Individual Stars*

V37, V49 and V42. These three stars display a very low amplitude in V. This has also been noted by diC11 and Clement et al. (2001). These stars are in the central regions of the cluster and therefore are very likely blended with near neighbours, so that their amplitudes appear diminished. None of them have proper motions reported in *Gaia*-DR3; thus, we cannot confirm their cluster membership.

V38, V41, V48, V51, V56, V69. These RRc variables are all blended in our images. They have no proper motions reported in *Gaia*-DR3, hence no membership status could be assigned.

V39. This double mode star was first found by Clement & Nemec (1990) with the periods $P_1 = 0.40704$ and $P_0 = 0.5465$. The fitting of our data with a model of these two periods is shown in Figure 11 and looks quite satisfactory given the intrinsic noise of our observations.

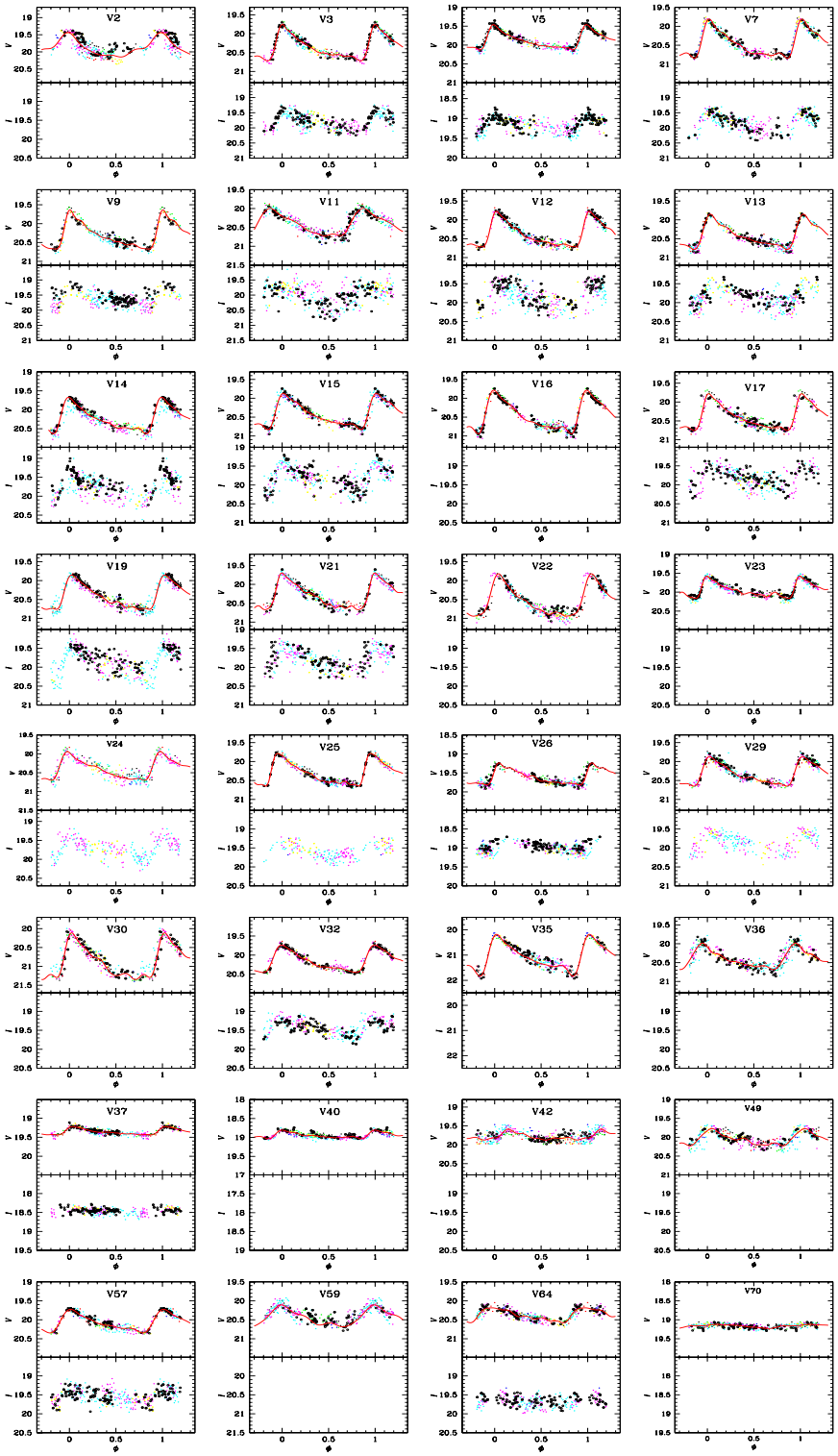

Fig. 7. Light curves of the RRab stars. Color code is as follows: black, red, green, blue, turquoise, lilac, yellow and empty circles for 2005, March 2007, April 2007, 2009, 2011-2012, 2013, 2017 and 2021-2022 seasons, respectively. The colour figure can be viewed online.

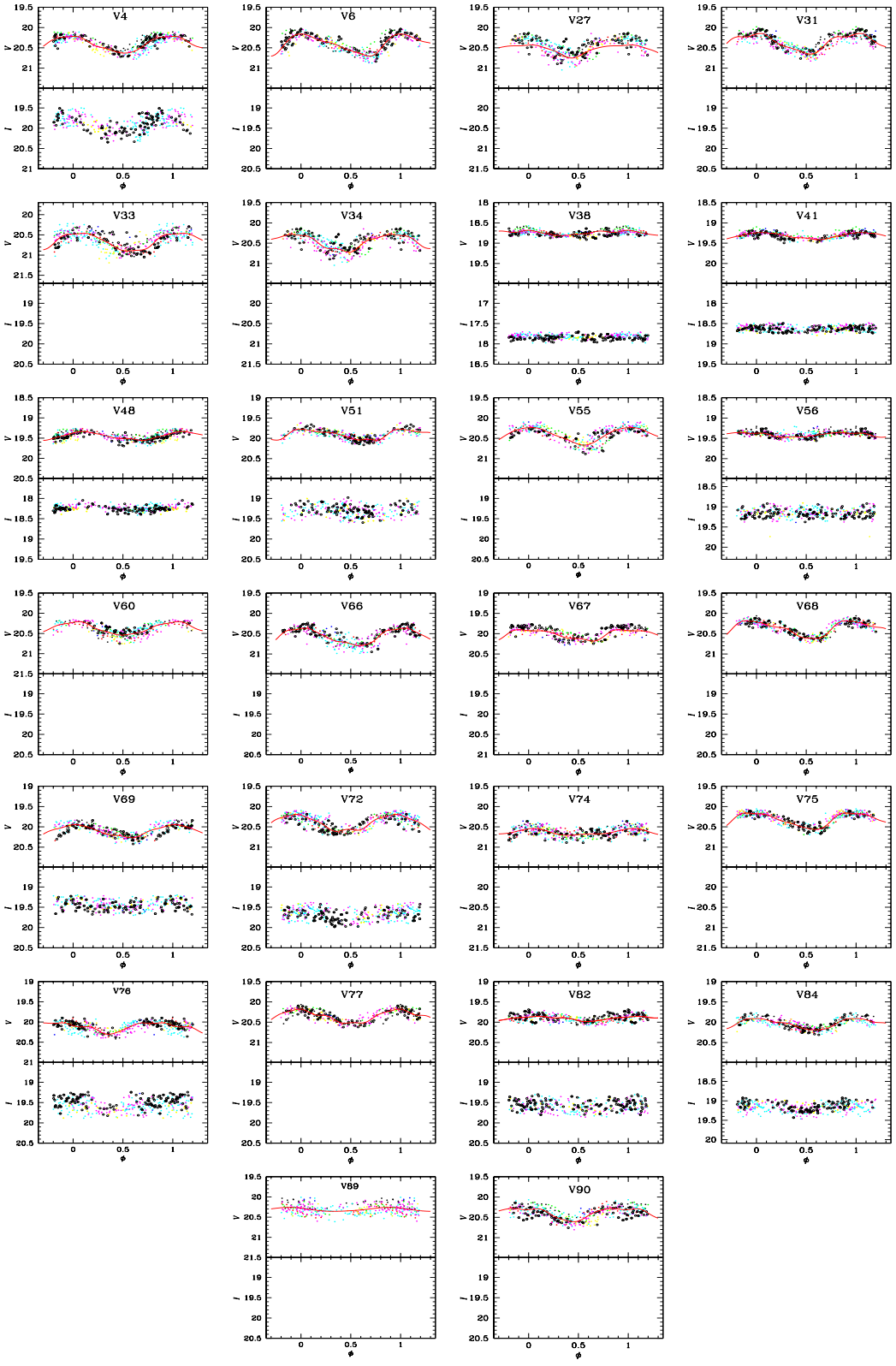

Fig. 8. Light curves of the RRc stars. Color code is as Figure 7. The colour figure can be viewed online.

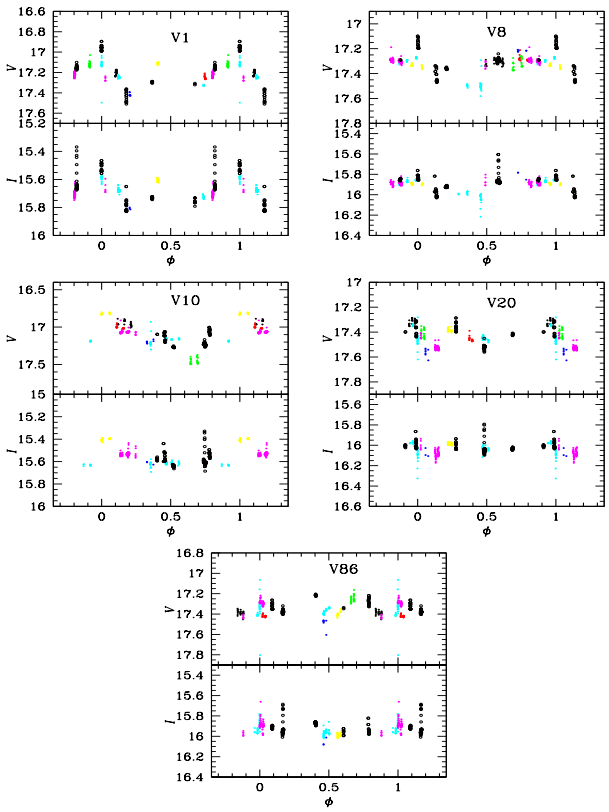

Fig. 9. Light curves of Long period variables in NGC 2419 phased with the periods of Table 2. Color code is as Figure 7. The colour figure can be viewed online.

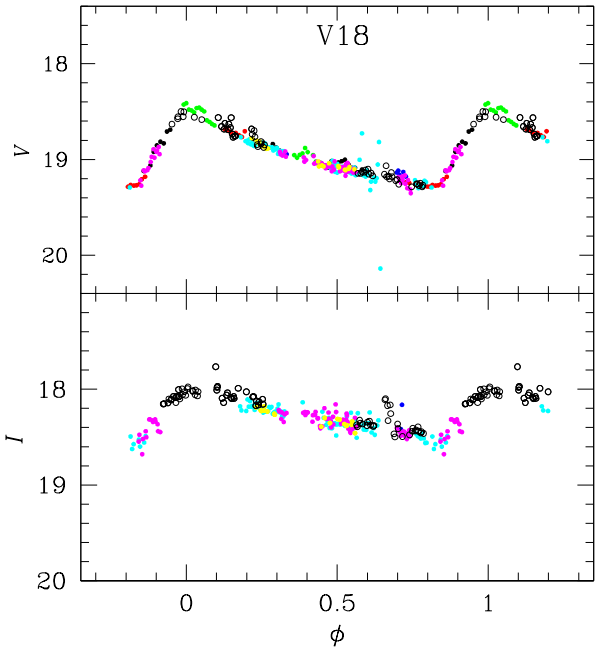

Fig. 10. Light curve of the CW star V18. The colour figure can be viewed online.

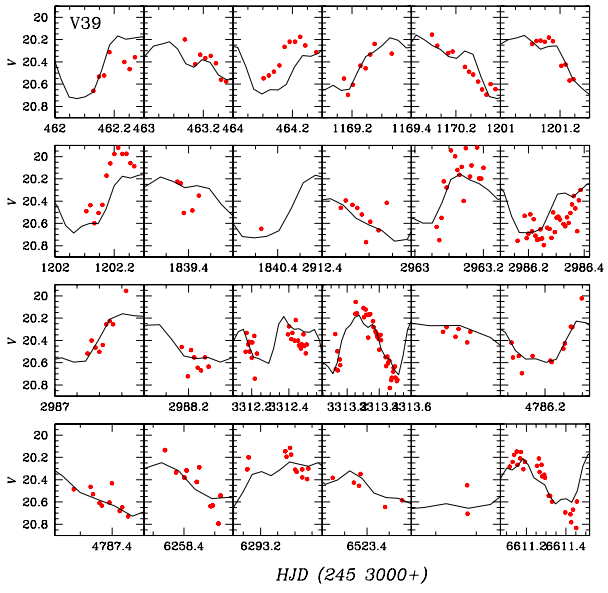

Fig. 11. Light curve of V39 with a two-period model fit with $P_0 = 0.54650$ and $P_1 = 0.40704$. The colour figure can be viewed online.

REFERENCES

Arellano Ferro, A. 2022, RMxAA, 58, 257, https://doi.org/10.22201/ia.01851101p.2022.58.02.08

_____. 2024, IAU Symposium, 376, At the crossroads of astrophysics and cosmology: Period-luminosity relations in the 2020s, ed. R. De Grijs, P. A. Whitelock, and M. Catelan, (CUP), 222, https://doi.org/10.1017/S1743921323002880

Arellano Ferro, A., Bustos Fierro, I. H., Calderón, J. H., & Ahumada, J. A. 2019, RMxAA, 55, 337, https://doi.org/10.22201/ia.01851101p.2019.55.02.18

Arellano Ferro, A., Figuera Jaimes, R., Giridhar, S., et al. 2011, MNRAS, 416, 2265, https://doi.org/10.1111/j.1365-2966.2011.19201.x

Arellano Ferro, A., Giridhar, S., & Bramich, D. M. 2010, MNRAS, 402, 226, https://doi.org/10.1111/j.1365-2966.2009.15931.x

Arellano Ferro, A., Luna, A., Bramich, D. M., et al. 2016, Ap&SS, 361, 175, https://doi.org/10.1007/s10509-016-2757-5

Arellano Ferro, A., Mancera Piña, P. E., Bramich, D. M., et al. 2015, MNRAS, 452, 727, https://doi.org/10.1093/mnras/stv1299

Arellano Ferro, A., Rojas Galindo, F. C., Bustos Fierro, I. H., et al. 2023, MNRAS, 519, 2451, https://doi.org/10.1093/mnras/stac3650

Baumgardt, H. & Vasiliev, E. 2021, MNRAS, 505, 5957, https://doi.org/10.1093/mnras/stab1474

Bono, G., Braga, V. F., Fiorentino, G., et al. 2020, A&A, 644, 96, https://doi.org/10.1051/0004-6361/202038191

Bono, G., Caputo, F., & Stellingwerf, R. F. 1994, ApJ, 423, 294, https://doi.org/10.1086/173806

Bramich, D. M. 2008, MNRAS, 386, 77, https://doi.org/10.1111/j.1745-3933.2008.00464.x

Bramich, D. M., Bachelet, E., Alsubai, K. A., Mislis, D., & Parley, N. 2015, A&A, 577, 108, https://doi.org/10.1051/0004-6361/201526025

Bramich, D. M., Figuera Jaimes, R., Giridhar, S., & Arellano Ferro, A. 2011, MNRAS, 413, 1275, https://doi.org/10.1111/j.1365-2966.2011.18213.x

Bramich, D. M., Horne, K., Albrow, M. D., et al. 2013, MNRAS, 428, 2275, https://doi.org/10.1093/mnras/sts184

Bustos Fierro, I. H. & Calderón, J. H. 2019, MNRAS, 488, 3024, https://doi.org/10.1093/mnras/stz1879

Cacciari, C., Corwin, T. M., & Carney, B. W. 2005, AJ, 129, 267, https://doi.org/10.1086/426325

Caputo, F., Castellani, V., & Tornambe, A. 1978, A&A, 67, 107

Carretta, E., Bragaglia, A., Gratton, R., D'Orazi, V., & Lucatello, S. 2009, A&A, 508, 695, https://doi.org/10.1051/0004-6361/200913003

Catelan, M. 2009, Ap&SS, 320, 261, https://doi.org/10.1007/s10509-009-9987-8

Clement, C. & Nemec, J. 1990, JRASC, 84, 434

Clement, C. M., Muzzin, A., Dufton, Q., et al. 2001, AJ, 122, 2587, https://doi.org/10.1086/323719

Deras, D., Arellano Ferro, A., Lázaro, C., et al. 2019, MNRAS, 486, 2791, https://doi.org/10.1093/mnras/stz642

Deras, D., Arellano Ferro, A., Bustos Fierro, I., & Yepez, M. A. 2022, RMxAA, 58, 121, https://doi.org/10.22201/ia.01851101p.2022.58.01.10

Di Criscienzo, M., Greco, C., Ripepi, V., et al. 2011, AJ, 141, 81, https://doi.org/10.1088/0004-6256/141/3/81

Gaia Collaboration, Vallenari, A., Brown, A. G. A., et al. 2023, A&A, 674, 1, https://doi.org/10.1051/0004-6361/202243940

Guldenschuh, K. A., Layden, A. C., Wan, Y., et al. 2005, PASP, 117, 721, https://doi.org/10.1086/431178

Kunder, A., Stetson, P. B., Cassisi, S., et al. 2013a, AJ, 146, 119, https://doi.org/10.1088/0004-6256/146/5/119

Kunder, A., Stetson, P. B., Catelan, M., Walker, A. R., & Amigo, P. 2013b, AJ, 145, 33, https://doi.org/10.1088/0004-6256/145/2/33

Landolt, A. U. 1992, AJ, 104, 340, https://doi.org/10.1086/116242

Pols, O. R., Schröder, K.-P., Hurley, J. R., Tout, C. A., & Eggleton, P. P. 1998, MNRAS, 298, 525, https://doi.org/10.1046/j.1365-8711.1998.01658.x

Pols, O. R., Tout, C. A., Schroder, K.-P., Eggleton, P. P., & Manners, J. 1997, MNRAS, 289, 869, https://doi.org/10.1093/mnras/289.4.869

Ripepi, V., Clementini, G., Di Criscienzo, M., et al. 2007, ApJ, 667, 61, https://doi.org/10.1086/522000

Schlafly, E. F. & Finkbeiner, D. P. 2011, ApJ, 737, 103, https://doi.org/10.1088/0004-637X/737/2/103

Schlegel, D. J., Finkbeiner, D. P., & Davis, M. 1998, ApJ, 500, 525, https://doi.org/10.1086/305772

Schröder, K.-P., Pols, O. R., & Eggleton, P. P. 1997, MNRAS, 285, 696, https://doi.org/10.1093/mnras/285.4.696

Silva Aguirre, V., Catelan, M., Weiss, A., & Valcarce, A. A. R. 2008, A&A, 489, 1201, https://doi.org/10.1051/0004-6361:200810047

Stetson, P. B. 2000, PASP, 112, 925, https://doi.org/10.1086/316595

Sturch, C. 1966, ApJ, 143, 774, https://doi.org/10.1086/148557

van den Bergh, S. & Mackey, A. D. 2004, MNRAS, 354, 713, https://doi.org/10.1111/j.1365-2966.2004.08228.x

VandenBerg, D. A., Bergbusch, P. A., Ferguson, J. W., & Edvardsson, B. 2014, ApJ, 794, 72, https://doi.org/10.1088/0004-637X/794/1/72

Yepez, M. A., Arellano Ferro, A., & Deras, D. 2020, MNRAS, 494, 3212, https://doi.org/10.1093/mnras/staa637

Yepez, M. A., Arellano Ferro, A., Deras, D., et al. 2022, MNRAS, 511, 1285, https://doi.org/10.1093/mnras/stac054

Zhang, T., Ramakrishnan, R., & Livny, M. 1996, ACM SIGMOD Rec., 25, 103, https://doi.org/10.1145/235968.233324

Zinn, R. & West, M. J. 1984, ApJS, 55, 45, https://doi.org/10.1086/190947

A. Arellano Ferro and M. A. Yepez: Instituto de Astronomía, Universidad Nacional Autónoma de México, Ciudad Universitaria, C.P. 04510, México.

I. Bustos Fierro: Observatorio Astronómico, Universidad Nacional de Córdoba, Córdoba C.P. 5000, Argentina.

G. A. García Pérez and G. Rios Segura: Facultad de Física, Universidad Veracruzana, Xalapa, México.

Sunetra Giridhar and S. Muneer: Indian Institute of Astrophysics, Bangalore, India.

M. A. Yepez: Instituto Nacional de Astrofísica, Óptica y Electrónica (INAOE), Luis Enrique Erro No.1, Tonantzintla, Pue., C.P. 72840, México.